J. Min. Metall. Sect. B-Metall. 59 (2) (2023) 327 - 338

Journal of Mining and Metallurgy, Section B: Metallurgy

IDENTIFICATION OF Fe-BEARING PHASES IN THE AS-CAST MICROSTRUCTURE OF AA6026 ALLOY AND THEIR EVOLUTION DURING HOMOGENIZATION TREATMENT

T. Radetić [a,*], M. Popović [a], M. Novaković [b], V. Rajić [b], E. Romhanji [a]

[a] University of Belgrade, Faculty of Technology and Metallurgy, Belgrade, Serbia
[b] University of Belgrade, Department of Atomic Physics, Vinča Institute of Nuclear Sciences – National Institute of the Republic of Serbia, Belgrade, Serbia

(Received 11 June 2023; Accepted 02 November 2023)

Abstract

The Fe-bearing intermetallic phases present in the as-cast AA6026 alloy and their evolution during homogenization treatments at 480-550°C were investigated using optical microscopy, SEM, and TEM techniques in combination with EDS analysis. In addition to the α-Al(Fe,Mn)Si phase with dendritic morphology, two types of plate-like Fe-bearing microconstituents were revealed in the microstructure of the as-cast alloy. The EDS microanalysis and electron diffraction showed that one set of platelets represented thin sections of α-Al(Fe,Mn)Si microconstituent. The other set of plate-like microconstituents was identified as a tetragonal, silicon-rich δ-Al_4(Fe,Mn)Si_2 phase. The formation of the δ-Al_4(Fe,Mn)Si_2 phase was attributed to the chemical composition of the alloy. During homogenization, the metastable δ-Al_4(Fe,Mn)Si_2 transformed into the α-Al(Fe,Mn)Si phase and fragmented. The dendritic α-Al(Fe,Mn)Si microconstituents underwent fragmentation. However, while the α-Al(Fe,Mn)Si microconstituents preserved a b.c.c. crystal lattice throughout the process, the product of the transformation of the δ-Al_4(Fe,Mn)Si_2 phase exhibited primitive cubic lattice.

Keywords: *6xxx alloys; Fe-bearing microconstituents; δ-Al_4(Fe,Mn)Si_2 phase; Homogenization; Phase transformation*

1. Introduction

Iron impurities are unavoidable in commercially available aluminum alloys. It has an extremely low solubility in solid aluminum, at most 0.05 wt.% at 650°C [1], and forms a series of intermetallic Al-Fe and Al-Fe-Si phases, which have a significant influence on further processing and the final properties of Al alloys [2-4]. In dilute alloy systems such as wrought 6xxx series alloys, the equilibrium Fe-bearing phase is α-AlFeSi [1] that has two crystallographic modifications. If the alloy contains no other transition metals but Fe, the stable phase has a hexagonal crystal structure, α_h-AlFeSi [5, 6]. Traces of transition metals such as Mn stabilize a cubic crystal structure, α_c-Al(Fe,Mn)Si [6, 7]. The cubic phase has a b.c.c. crystal lattice (Im$\underline{3}$, a= 1.256 nm) and varied stoichiometry with Fe/Si ratio in a range of 1.5-3 [8, 9]. The α-Al(Fe,Mn)Si microconstituents adopt different morphologies, from Chinese script to polyhedral [10]. Another phase commonly found in 6xxx type of alloys is metastable β-Al_5FeSi. The β-Al_5FeSi has a monoclinic crystal lattice (a=b=0.612 nm, c=4.15, β=91°), and its morphology consists of a network of interconnected thin plates at the grain boundaries and interdendritic channels [11]. The presence of β-Al_5FeSi microconstituent in microstructure is detrimental to the properties and processing of the alloys. Poor cohesion of β-Al_5FeSi microconstituents to the surrounding aluminum matrix combined with sharp faceted interfaces can lead to local crack initiation and low ductility of as-cast billets of the 6xxx alloys. A propensity toward hot cracking and surface defects such as pickup is linked to the incipient melting of β-Al_5FeSi phase platelets during hot working [12].

The phase selection and formation of α-AlFeSi and β-Al_5FeSi phase microconstituents during solidification are influenced by a number of factors. It has been established that high content of Fe or other transition metals and high cooling rates can suppress the formation of β-Al_5FeSi during solidification [9, 13, 14].

Besides microsegregation removal and dissolution of Mg_2Si microconstituents, the transformation of Fe-bearing microconstituents into a more workable form takes place during the homogenization treatment of 6xxx alloys at temperatures of 450 – 580 °C. β-

Corresponding author: tradetic@tmf.bg.ac.rs

https://doi.org/10.2298/JMMB230611028R

Al_5FeSi platelets transform into strings of less interconnected, rounded α-Al(Fe,Mn)Si particles [11]. The transformation significantly improves the hot workability and surface quality of 6xxx alloys [15,16]. The α-Al(Fe,Mn)Si also binds less silicon enriching the Al–matrix with Si and increasing the aging potential of an alloy.

Due to its technological importance, microstructure evolution during homogenization has been extensively studied experimentally [11, 16-20] as well as in combination with modeling [21-27]. Most of the attention has been directed toward β-Al_5FeSi→α-AlFeSi transformation, whose completion, due to its sluggish kinetics, determines the optimal homogenization procedure. The additions as small as 0.02 mas% of Mn increase the rate of β-Al_5FeSi→α-AlFeSi transformation, and with further increase in manganese content up to 0.2 mas%, it continues to speed up [15, 22]. The transformation mechanism was investigated by both ex-situ [22, 23] and in-situ experiments [7,8]. It has been established that preferential sites for α-AlFeSi phase nucleation are basal Al / β-Al_5FeSi interface and Mg_2Si particles in the vicinity of β-Al_5FeSi [7, 8, 22, 23]. The α-AlFeSi phase growth appears to be controlled by Fe diffusion, whether volume [22, 23] or interface [7, 8] but capillary effects also have a role in the transformation [7].

The evolution of the α-AlFeSi microconstituent during homogenization has been less studied by far [5, 11] as that phase is considered less detrimental for properties and processing. There is also scant research on other Fe-bearing phases [9, 20], although iron can form over fifteen intermetallic compounds in the Al-Fe-Mg-Si system. However, conditions for their formation and evolution during the homogenization of 6xxx alloys gain relevance as the alloys' composition becomes more complex with the increased use of recycled material for wrought aluminum alloy production as well as the development of new alloys.

The alloy AA6026 belongs to a group of free-cutting alloys [28-30] and, as such, contains the low melting point metals Pb and Bi. Essentially insoluble in Al [2], Pb and Bi form particles at grain boundaries which, due to poor cohesion to the Al-matrix and low melting point, should be detrimental to the ductility at room and, especially, at elevated temperatures. However, previous research [31] showed that the effect of Pb and Bi on the alloy's ductility becomes prominent only after the large fraction of plate-like Fe-bearing phases transformed into rounded α-Al(Fe,Mn)Si particles during the high-temperature homogenization, highlighting the impact of Fe-bearing phases and their transformations on the alloy properties.

The chemical composition of AA6026 is derived from highly alloyed AA6082, and, in addition to low melting point metals, it can contain various transition metals as alloying elements. This study objective was to characterize the phase composition of the Fe-bearing microconstituents in the as-cast state of the alloy AA6026 and to investigate the evolution of Fe-bearing phases other than β-Al_5FeSi during homogenization in the 480-550 °C temperature range. Various microstructural characterization techniques, including optical microscopy (OM), scanning electron microscopy (SEM), EDS microanalysis, and transmission electron microscopy with diffraction (TEM/SAD), were applied to characterize Fe-bearing microconstituent morphology and identify their crystal structure and phase composition.

2. Experimental

An industrially DC cast billet of AA6026 alloy, supplied by NISSAL Aluminium Extrusion Plant – Serbia, was used in this study. The chemical composition of the alloy is given in Table 1.

The billet diameter was 200 mm, and samples for the investigation were sectioned from the region 50 mm from the billet surface. The as-cast material was subjected to three homogenization regimes: 12h / 480°C, 12h / 530°C, and 6h / 550°C.

The optical (OM), scanning (SEM), and transmission electron microscopy (TEM) techniques were used for microstructural characterization. The samples for OM were mechanically polished by standard metallographic procedures and electrolytically etched in Barker's reagent. The grain and dendrite microstructure of the as-cast and homogenized samples was assessed in a bright field and polarized light modes. Mechanically polished specimens were characterized in FEG SEM/EDS FEI Scios 2 Dual Beam electron microscope at 15 kV. The microconstituents' morphology was examined in chemically sensitive electron back-scattered mode (BSE), while energy dispersive spectroscopy (EDS) was used for semi-quantitative chemical analysis. Further characterization of the microconstituents and identification of their crystal structure was conducted in a transmission electron microscope (TEM) by a combination of conventional bright (BF) and dark field (DF) imaging, selected area diffraction (SAD), high annular dark field (HAADF) imaging and EDS elemental mapping. Samples for TEM were prepared in PIPS Gatan ion-mill under conditions of 2.7 keV and 3 rpm in 5.0 argon. TEM characterization was conducted in the FEI Talos F200X microscope equipped with the EDS detector at 200 kV.

Table 1. *Chemical composition of the studied AA6026 alloy / wt.%*

Si	Fe	Cu	Mn	Mg	Cr	Ti	Pb	Sn	Bi	Zr
1.125	0.097	0.294	0.487	1.033	0.123	0.009	0.252	0.006	0.697	<0.001

3. Results

3.1. As-cast state

Figure 1 shows OM micrographs of the anodized microstructure of the AA6026 alloy in the as-cast state. The grains have dendritic equiaxed morphology with the mean grain size and secondary dendrite arms spacing (DAS) of 140 μm and ≈31 μm, respectively. The microconstituents are located at the cell and grain boundaries, as seen in Figure 1b. Based on the relation between the cooling rate and measured DAS, $V=3.57\times10^{4}DAS^{-2.56}$ [11, 14], the estimated cooling rate was 5.4 Ks^{-1}.

SEM/EDS characterization of microstructure showed that, due to the complex chemical composition of the AA6026 alloy (Table 1), there were microconstituents such as low melting point elements (Pb and Bi) particles and Q-AlMgCuSi intermetallic besides Fe-bearing microconstituents and Mg_2Si common to Al-Mg-Si alloys (Figure 2a). The microconstituents other than Fe-bearing phases are described elsewhere [31]. Although Fe-bearing microconstituents had a range of morphologies: dendritic (Figure 2a), Chinese script, and thin plates, the plate-like particles prevail (Figure 2b). Based on the literature [10] and the EDS characterization, microconstituents with dendritic and Chinese script morphology were attributed to α-Al(Mn,Fe)Si phase. The microconstituents with thin plate morphology underwent a more thorough examination.

The results of the EDS analysis of the specimens in the as-cast state and after homogenization are shown in Figure 3. EDS microanalysis has been frequently employed to identify various Al-Fe(Mn)-Si phases by comparing the measured (Fe+Mn)/Si ratio to values inferred from the intermetallic compounds' stoichiometry [6, 26, 32, 33]. Rather than as a simple ratio for individual particles, the (Fe+Mn)/Si ratio was determined by applying a linear fit to the sets of the ((Fe+Mn+Cr)at%, Si at%) points representing the composition of different microconstituent particles (Figures 3a-d). The approach proposed by [34] minimizes the effect of the part of the EDS signal arising from the aluminum matrix and provides a more accurate (Fe+Mn)/Si ratio.

Figures 3a and e show the results of EDS analysis for plate-like microconstituents in the as-cast state. It is clear from the plots that there were two populations of microconstituents. A linear fit to one set of the platelets (black squares in Figures 3a and b) showed (Fe+Mn+Cr)/Si ratio of k=1.53 that agreed with $Al_{15}(Fe,Mn)_3Si_2$ stoichiometry of cubic α_c-Al(Fe,Mn)Si. The manganese content in those microconstituent particles was higher than iron's, as can be seen from the plot in Figure 3e. The (Fe+Mn+Cr)/Si ratio for another set of the plate-like microconstituents (red circles in Figures 3a and e) was k=0.3 (Figure 3a), which was far below the value of 1 expected for the β-Al_5FeSi phase. The stoichiometry of the δ-Al_4FeSi_2 phase with a Fe/Si ratio of 0.5 appeared closer, although still higher than the obtained value. Frequent observations of the Mg_2Si

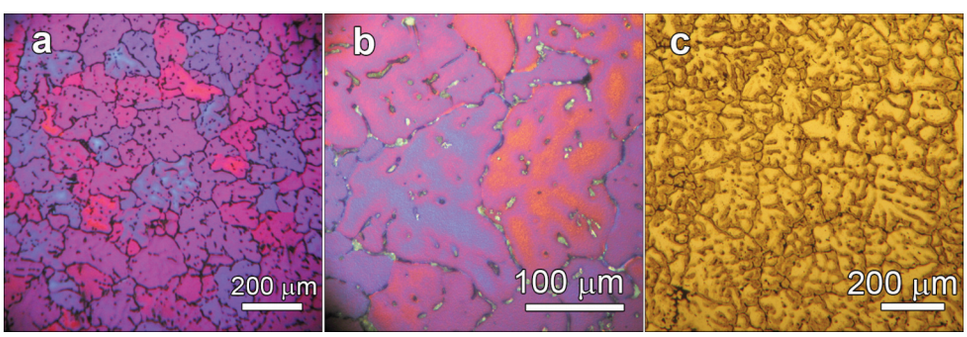

Figure 1. *Optical micrographs of the grain and dendrite microstructure in the as-cast state: (a-b) polarized light; (c) bright field*

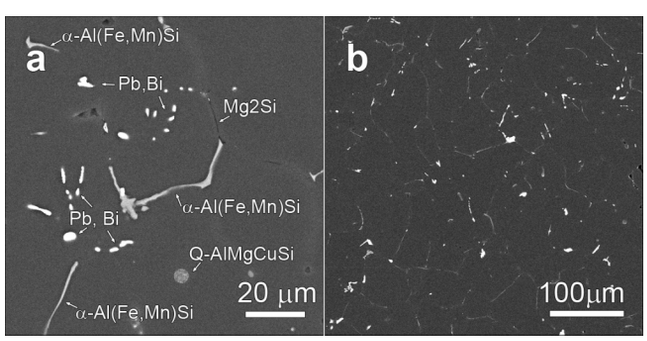

Figure 2. *BSE SEM micrographs of the as-cast state microstructure showing various types of microconstituents*

phase attached to the interface of the Fe-bearing platelets (Figures 4c and d) might suggest that high Si content was due Mg_2Si. However, the EDS spectra from the plate-like phase showing higher Mg content than one in the Al-matrix were excluded from the analysis to avoid the eventual contribution of Mg_2Si to the EDS signal.

The second set of plate-like microconstituents also contained manganese, although less than iron with (Mn+Cr)/ Fe = 0.7 (Figure 3e). The detection of the Mn in a microconstituent has been frequently used to rule out the β-Al_5FeSi phase under the assumption that it cannot contain manganese [9, 10, 22, 23]. While that assumption has been challenged by the recent study [7], the measured Mn fraction in the microconstituent platelets exceeded one reported more than twice (Mn/Fe≈0.7- vs- ≤0.3 in [7]), rendering them unlikely to be a β-Al_5FeSi phase. On the other hand, the δ-$AlFeSi_2$ phase can incorporate manganese in a wide range [35-38].

Apart from both having form of thin plates, closer examination revealed distinct morphological features of each set (Figure 4). The microconstituent with (Fe+Mn+Cr)/Si ratio corresponding to the cubic phase tended to consist of individual plates with interfaces bending along the grain boundary (Figure 4a). In contrast, microconstituents of another set were bundles of platelets that grouped and delineated grain boundaries and interdendritic space (Figure 4b). The individual particles had the form of long thin plates with flat, faceted edges (Figures 4c-d). Such morphology is typical for both

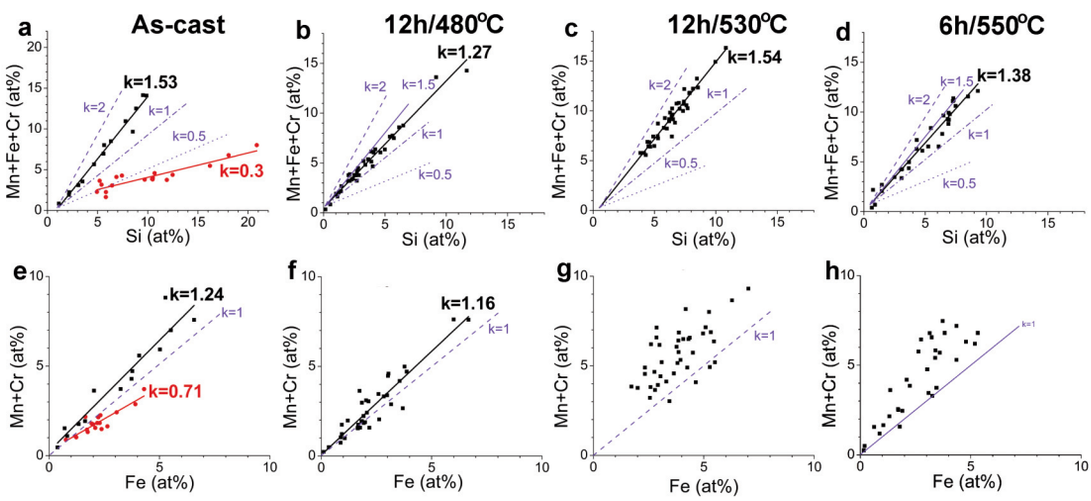

Figure 3. *SEM/EDS analysis of the chemical composition of the plate-like microconstituents in the as-cast state and after the homogenization treatments in the 480-550°C temperature range: (a-d) Plots of (Fe+Mn+Cr) at%-vs-Si at%; (e-h) Plots of (Mn+Cr) at%-vs-Fe at%*

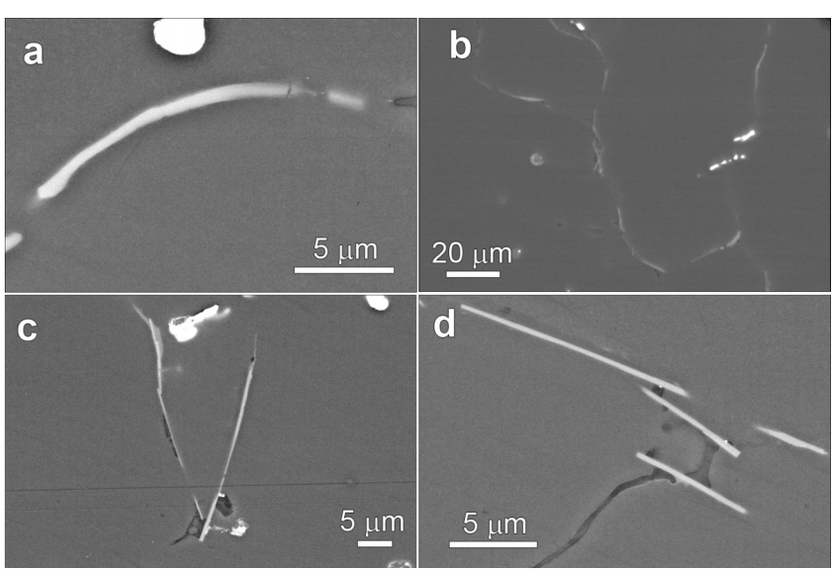

Figure 4. *BSE SEM micrographs of the plate-like microconstituents in the as-cast state: (a) the phase with (Fe+Mn+Cr)/Si=1.53; (b-d) the phase with (Fe+Mn+Cr)/Si=0.3*

β-Al_5FeSi and δ-Al_4FeSi_2 phases making metallographic differentiation difficult; in older literature, both phases were labeled as β-phase [35] regardless of differences in crystal structure and stoichiometry.

CTEM/SAD characterization confirmed that two sets of plate-like microconstituents were different intermetallic compounds. The thin microconstituent shown in Figure 5a was not strongly faceted and had a slightly curved shape that followed the grain boundary. The indications of SEM/EDS analysis that microconstituents with such morphology were cubic α-Al(Fe,Mn)Si phase was confirmed by diffraction. The SAD pattern of the microconstituent (Figure 5b) was consistent with a [001] zone axis of b.c.c. crystal structure and determined interplanar spacing correspond to α-Al(Fe,Mn)Si phase.

A BF image of the other type of microconstituent with long straight facets and a series of diffraction patterns obtained over a wide range of tilts is shown in Figure 6. The microconstituent consisted of multiple plates which, to accommodate grain boundary curvature, formed an angle rather than bended into a curve consistent with SEM observations. SAD patterns shown in Figures 5b-d were indexed as [10], [10], and [20] zone axis of the δ-Al_4FeSi_2 phase with the tetragonal crystal structure. The angles between zones, the angles between planes, and interplanar spacing in each zone axis were consistent with the published crystallographic data for the δ-Al_4FeSi_2 phase (a= 0.615 nm and c=0.947 nm) [35-40]. The presence of extra-reflections such as (001), (31), and (120) suggested the P type of Bravais lattice [36, 40]. However, the presence of multiple plates (Figure 6a) along with a weak intensity of extra-reflections, e.g. (001) reflections in [100] zone axis could be detected only on the intensity profile (Figure 6c), which suggested that the extra-reflections originate from the stacking faults or twinning and that the lattice was actually body-centered (I4/mcm) as proposed by [40].

STEM imaging and elemental mapping (Figure 7) confirmed that the δ-Al_4FeSi_2 phase contained Mn and Cr beside Fe. Semi-quantitative analysis showed that the (Fe+Mn+Cr)/Si ratio in the microconstituent was ≈0.6, which was closer to the stoichiometric value of 0.5 than the results of SEM/EDS analysis. Traces of Cu and Mg at the constituent plate/matrix interface were attributed to the Q-phase [41].

Low-melting point elements, Pb and Bi, particles were occasionally observed as bright pearls attached to the interfaces of Fe-bearing microconstituents (Figures 4c-d), but no traces of the elements were detected within microconstituents.

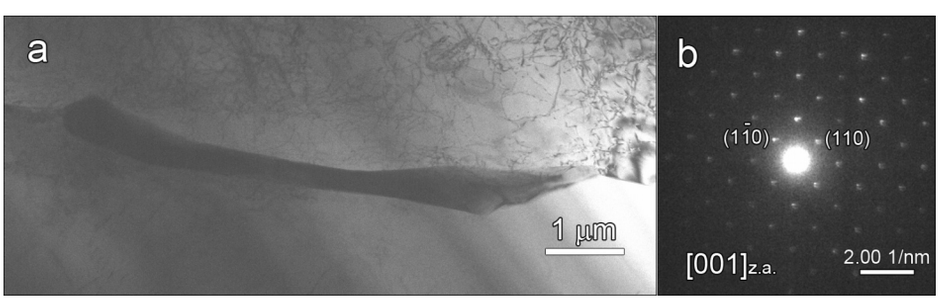

Figure 5. *(a) BF TEM micrograph of the Fe-bearing microconstituent; (b) Corresponding SAD pattern. With the microconstituent in $[001]_{z.a.}$ orientation, the diffraction pattern exhibits reflection of b.c.c. α-Al(Fe,Mn)Si*

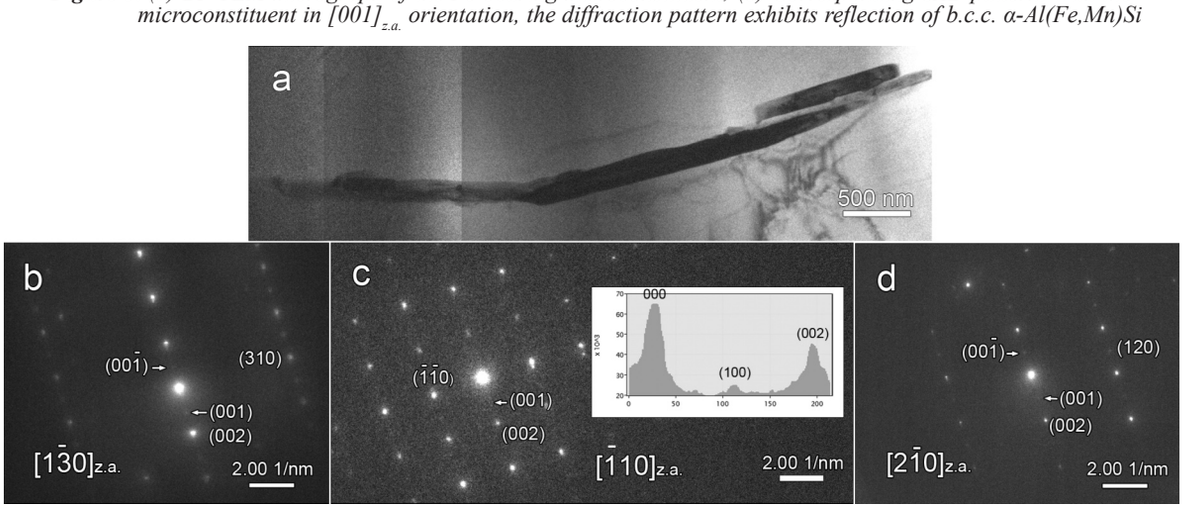

Figure 6. *(a) BF TEM micrograph of the strongly faceted Fe-bearing microconstituent; (b-d) Corresponding SAD patterns under different tilts are indexed as [10], [10], and [20] zone axis of δ-$Al_4(Fe,Mn)Si_2$*

3.2. Homogenization

Homogenization treatments lead to compositional and morphological changes in the microconstituents. The distinction in the chemical composition between the two types of plate-like microconstituents vanished after homogenization at the lowest temperature, 480 °C. As seen in Figure 3b, the points in the (Fe+Mn+Cr) at%-vs-Si at% plot converged toward a single straight line with the (Fe+Mn+Cr)/Si ratio of k=1.27. Although that value did not correspond to any of the established stoichiometry of Fe(Mn)- bearing phases, it indicated the transformation of the δ-Al_4FeSi_2 phase. Homogenization at higher temperatures, i.e., 530 °C and 550 °C, resulted in values of Fe+Mn+Cr)/Si ratio closer to the stoichiometric value of 1.5 for $Al_{15}(Fe,Mn)_3Si_2$ (Figures 3c-d) and further increase in Mn and Cr content in the microconstituents (Figures 3g-h).

Figure 8 shows the morphological transformations of the microconstituents during the homogenization treatment. The microconstituents whose geometry resembled one of the δ-Al_4FeSi_2 phase in the as-cast state, i.e., a bundle of straight plates, were characterized by rough interfaces after homogenization at lower temperatures (Figure 8a-b). That was a striking change from the long, flat facets of the as-cast state (Figures 4b-d). Furthermore, as shown in Figure 8b, the parts of the plates underwent fragmentation during homogenization at 480 °C. Fragmented particles remained elongated, while uneven contrast within microconstituent plates suggested dissolution. The homogenization at 530 °C had a similar effect, although a fraction of fragmented microconstituents increased to about 50-70%. The thinnest sections of α-Al(Fe,Mn)Si microconstituents, whether of plate-like or dendritic morphology, also began to fragment at 480 °C, but extensive degradation of the microconstituent occurred during homogenization at 530 °C (Figure 8c). The fragmented parts of the microconstituent with dendritic morphology tended to have a coarser, more irregular shape than fragmented plate-like microconstituents, in agreement with previous reports [11, 20]. At the highest homogenization temperature, 550 °C, over 90% of the microconstituents underwent fragmentation, followed by extensive spheroidization that resulted in desired pearl-necklace morphology (Figure 8d).

TEM characterization was conducted in order to identify the phase composition of the microconstituents after homogenization. BF image of dendritic α-Al(Fe,Mn)Si microconstituent that started to disintegrate and corresponding diffraction patterns are shown in Figure 9. The SAD indexing and the fact that the shortest g-vector in [10] zone axis was (110) showed consistency with the b.c.c. crystal lattice.

A more complex configuration of the microconstituents is shown in Figure 10.

A string of fragmented particles, having a lenticular and cylindrical shape, was connected by a ≈0.5 μm thin strip that broadened into ≈1.5 μm thick ribbon-like microconstituent with irregular boundaries, as seen in the lower part of the micrograph. The SAD patterns of the microconstituent (Figures 10c and d) were indexed as [3] and [01] zone axes of the cubic lattice. The lattice parameter of a= 1.26 nm corresponded to the α-Al(Fe,Mn)Si. However, {100} type reflections in the SAD pattern indicated primitive lattice righter than

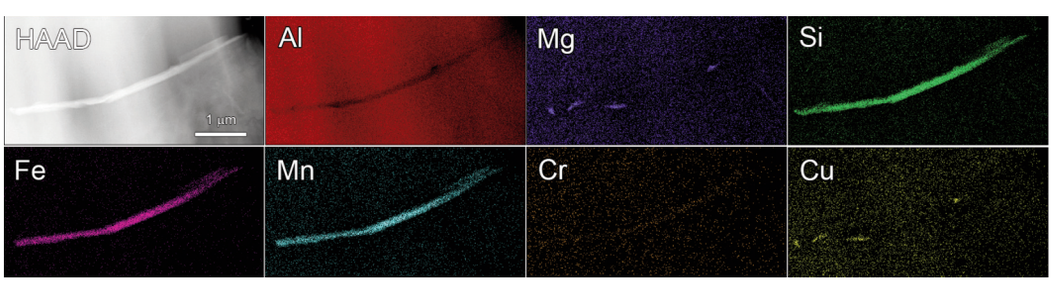

Figure 7. *STEM image and EDS elemental maps of the δ-$Al_4(Fe,Mn)Si_2$ platelets shown in Figure 6*

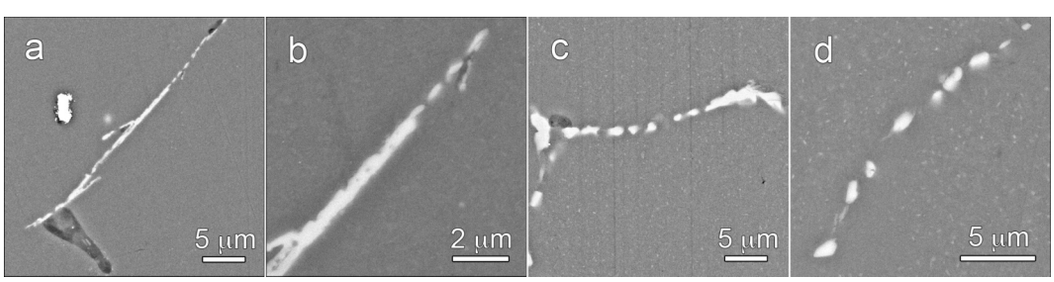

Figure 8. *BSE SEM micrographs of the Fe-bearing microconstituents after homogenization treatment at (a-b) 12h at 480°C; (c) 12h at 530°C; (d) 6h at 550°C*

the b.c.c. The SAD patterns of the particles showed the same crystal structure. There was only a small disorientation between ribbon-like microconstituent and particles, as seen in diffraction patterns recorded under the same tilt (inserts in Figure 10a). Although the rest of the particles showed in the micrograph had similar orientations, they did not lighten up in the DF images due to the excessive thickness. HAADF/EDS maps (Figure 11) did not reveal differences in the chemical composition between the microconstituent and the particles, as both contained Fe, Mn, and Cr, with Mn+Cr/Fe>1.

The orientation of the neighboring particles forming the string configuration was not necessarily the same as seen in the dark field micrograph and corresponding diffraction patterns shown in Figure 12. However, diffraction patterns of fragmented particles always revealed the presence of {100} type reflections, a signature of the primitive lattice.

4. Discussion

The presence of non-equilibrium constituent phases in DC cast aluminum alloys is a norm [4, 41]. During solidification, the elements with low partition coefficients, such as Fe and Si, segregate into liquid interdendritic regions, enriching the melt and giving rise to various variant and invariant reactions [42, 43]. In the wrought 6xxx alloys, besides the equilibrium α-Al(Fe,Mn)Si phase, a plate-like β-Al_5FeSi phase is expected to form [9, 11, 44]. However, microstructural characterization of the studied AA6026 alloy did not reveal the β-Al_5FeSi phase but δ-Al_4FeSi_2 (Figures 3 and 6) as a plate-like constituent

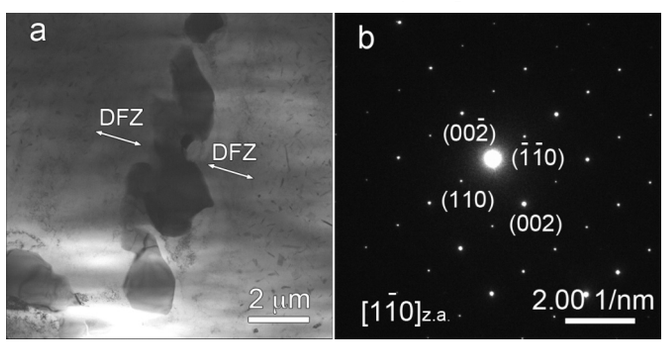

Figure 9. *(a) BF TEM micrograph of the dendritic α-Al(Fe,Mn)Si microconstituent after homogenization 12h at 530°C. Acronym DFZ stands for dispersoid free zones; (b) $[10]_{z.a.}$ SAD pattern of the α-Al(Fe,Mn)Si phase*

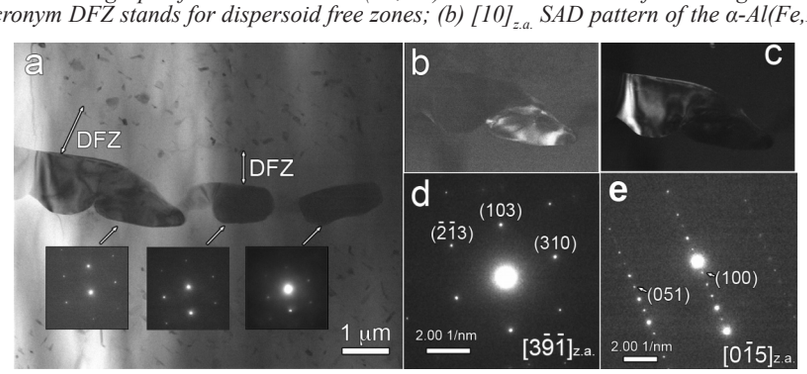

Figure 10. *(a) Bright-field TEM micrograph of the complex microconstituent configuration after homogenization 12h at 530°C. Inserted diffraction patterns indicate small disorientation between fragments; (b-c) Corresponding dark-field TEM micrographs of the microconstituent fragments; (d-e) SADs patterns under different tilts indexed as [3] and [01] zone axis of the simple cubic α-Al(Fe,Mn)Si phase*

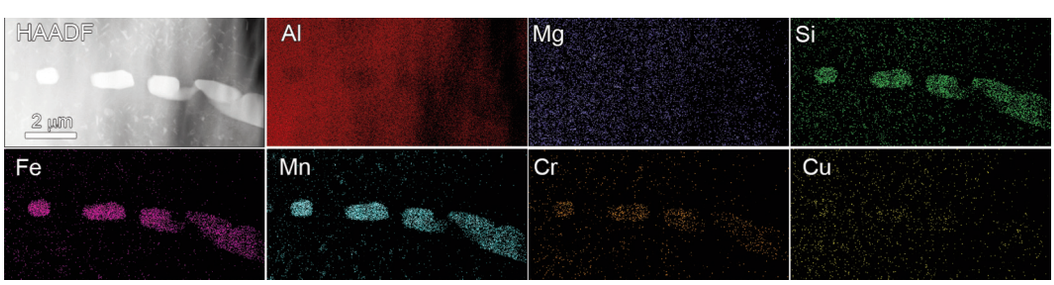

Figure 11. *STEM image and EDS elemental maps of the microconstituent shown in Figure 10. Annealed for 12h at 530°C*

in the as-cast state. δ-Al_4FeSi_2, the phase with high silicon content, is known to form in Al-Si casting alloys [35-40] but is unlikely in wrought Al-Mg-Si alloys. Yet, plate-like microconstituents with (Fe+Mn+Cr) /Si ratio close to 0.5, which correlated with the stoichiometry of the δ-Al_4FeSi_2 phase, and were also reported in [32, 45].

Constituent phase selection is sensitive to solidification parameters such as cooling and growth rate as well as alloy chemistry [9, 13, 14, 21]. At low cooling rates, the β-Al_5FeSi phase can form, while an increase in cooling rate favors α-Al(Fe,Mn)Si [14] or, at even higher rates, can lead to the formation of metastable phases like π-AlMgFeSi [20]. Rapid cooling also stabilizes the δ-$Al_4(Fe,Mn)Si_2$ phase in Al-Si alloys with high Si content; otherwise, it transforms into α-Al(Fe,Mn)Si or β-Al_5FeSi [38]. However, the estimated cooling rate of 5.4 Ks^{-1} for the characterized section of the DC bullet is sufficiently low to allow for β-Al_5FeSi phase formation [14], suggesting the alloy's chemical composition as a controlling factor for the phase selection.

In the Al-rich part of the ternary Al-Fe-Si system [1,43], intermetallic phase selection is determined by Fe/Si ratio. Al_3Fe and δ-Al_4FeSi_2 phases can form if Fe/Si ratio is high and low, respectively, while α-Al(Fe,Mn)Si and β-Al_5FeSi phases are stabilized in intermediate range of Fe/Si. The excess Si and very low Fe content (≤0.1 wt%) are shared features of the alloy under study and other alloys having intermetallic phases with Fe/Si ≈0.5 [32, 45]. Such chemistry could be responsible for the enrichment of the residual liquid with Si and a sufficiently low Fe/Si ratio to favor the formation of the Si-rich intermetallic phase like δ-Al_4FeSi_2. However, Sweet et al. [9] detected the β-Al_5FeSi phase in the alloy with a similar, low Fe content (0.1 wt%).

A review of the alloys' chemical composition (Table 2) points out that, in addition to Fe/Si ratio, the phase selection depends on the content of other transition metals and the ability of a phase to incorporate them into its crystal lattice. β-Al_5FeSi, which contains no or only small amounts of Mn [7], tends to form in alloys with little or no manganese, such as in [9]. On the other hand, in δ-$Al_4(Fe,Mn)Si_2$ phase, transition elements Mn and Cr can substitute for Fe in the crystal lattice [35-38]. Apparently, in the alloys with the combination of high Mn(+Cr) content with high Si and low Fe (Table 2), the δ-$Al(Fe,Mn)Si_2$ phase is favored over β-Al_5FeSi.

However, the formation of silicon-rich δ-$AlFeSi_2$ phase in 6xxx alloys would require significant deviation in the local chemistry of the residual melt from the nominal alloy composition during the solidification. The distribution of microconstituents reflects the effect of the local chemistry of interdendritic channels. δ-$AlFeSi_2$ platelets are usually observed in groups that delineate grains, as shown in Figure 5. On the other hand, observations of α-Al(Fe,Mn)Si and δ-$Al(Fe,Mn)Si_2$ microconstituents lying along the same grain boundary or interdendritic channel were rare. The formation of Mg_2Si at δ-$AlFeSi_2$ interfaces indicates the further enrichment of residual liquid with Si as Mg_2Si forms at later stages of the solidification.

Considering that the δ-$Al(Fe,Mn)Si_2$ is not a stable phase in dilute Al-Mg-Si systems such as 6xxx series alloys, it is expected to transform during homogenization treatment. In Al-Si and Al-Fe-Si alloys, δ-$Al(Fe,Mn)Si_2$ transforms either into β-Al_5FeSi or α-Al(Fe,Mn)Si during the solidification process [37, 38] and β-Al_5FeSi during subsequent heat treatment [46]. Indeed, morphological changes, such as platelet fragmentation and interface roughening, as

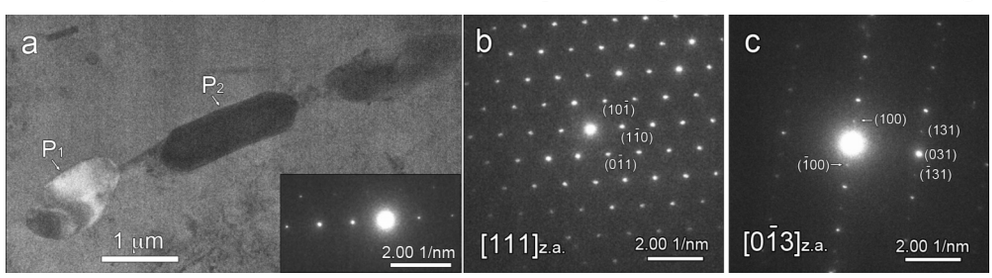

Figure 12. *(a) DF TEM micrograph of the string of particles after homogenization for 6 h at 550°C; (b) SAD of the particle P_1 in $[111]_{z.a.}$ orientation; (c) SAD of the particle P_2 under same tilt shows $[03]_{z.a.}$ orientation. The presence of (100) reflections indicates a primitive cubic lattice*

Table 2. *Chemical compositions of the studied alloy and alloys in other studies that had Fe/Si≤0.1 / wt%*

	Si	Fe	Cu	Mn	Mg	Cr	Ti	Zr	Zn	Pb	Bi
study	1.125	0.097	0.294	0.487	1.033	0.123	0.009	<0.01	/	0.252	0.697
[32]	1.15	0.068	0.145	0.28	0.50	0.175	0.018	/	/	/	/
[45]	0.85	<0.01	0.20	0.1	0.66	/	/	0.12	0.60	/	/
[9]	0.52	0.09	0.35	<0.001	0.35	/	0.05	/	/	/	/

well as EDS analysis indicate the transformation occurring during homogenization. The results of EDS analysis (Figures 3a-c), i.e., a change from two branches present in the plot for the as-cast state to a single after homogenization and derived (Fe+Mn+Cr)/Si ratios, signal the δ-Al(Fe,Mn)Si_2 phase transformation even at the lowest homogenization temperature of 480 °C. There is ambiguity about whether β-Al_5FeSi or α-Al(Fe,Mn) is the product of the transformation at 480 °C since the (Fe+Mn+Cr)/Si ratio of 1.27 (Figure 3b) corresponds to the stoichiometry of neither of them. However, a similar (Fe+Mn+Cr)/Si ratio was observed in the α-Al(Fe,Mn)Si phase, already known for varied stoichiometry [8-10], formed by the peritectic reaction of δ-Al(Fe,Mn)Si_2 and liquid during solidification of Al-Si alloys [38]. In addition, the δ-Al(Fe,Mn)Si_2 platelets contained a substantial fraction of Mn and Cr (Figures 3a,e and 6). Hence, the transformation into β-Al_5FeSi should involve the release of Mn (+Cr) into the aluminum matrix surrounding the microconstituents since the β-Al_5FeSi phase does not favor transition metal elements other than Fe. Yet, the results of microstructural characterization show the opposite behavior. The formation of dispersoid-free zones (DFZ) in the microconstituents' vicinity (Figures 9 and 10) clearly indicates that Mn depletion occurred in those regions during the homogenization. The mean width of DFZ, being in a range of 1.7- 2.5 μm for homogenization at 480 °C – 550 °C [31], is close to the Mn diffusion length at temperatures of interest ($\delta \approx 1.47\text{-}2.07$ μm for τ=6-12 h at 500 °C with $D_{Mn} \approx 1\times10^{-16} m^2 s^{-1}$ [21]). Moreover, the results of EDS microanalysis showed that Mn+Cr fraction in microconstituents increased after homogenization treatment (Figures 3e-h). Apparently, manganese diffused toward microconstituents, where it was consumed during the transformation of the δ-AlFeSi phase, leaving Mn-poor zones behind.

Supply of Mn and Cr from DFZ introduced ordering reaction into phase transformation of δ-Al(Fe,Mn)Si_2. Like previous reports [7,8,43], diffraction patterns of the α-Al(Fe,Mn)Si microconstituents showed the b.c.c. structure in the as-cast state as well as after the disintegration during homogenization treatments. However, the diffraction patterns of the products of δ-Al(Fe,Mn)Si_2 phase transformation (Figures 10 and 12) contained reflections characteristic of the primitive variant of cubic α-Al(Fe,Mn)Si lattice. Frequently observed in dispersoids if Mn/Fe ratio was high [47, 48], but not in microconstituents, the primitive cubic cell (P) was indicative of the ordering of Fe and Mn atoms within the lattice.

It is important to emphasize that there was no difference in the composition of the remaining platelets and the fragmented particles. Similarly, TEM characterization showed that the ribbon-like microconstituent, whose morphology corresponded to platelets with rough interfaces observed by SEM, and surrounding fragmented particles had the same cubic crystal structure and displayed a small disorientation. It appears that the transformation of δ-Al_4(Fe,Mn)Si_2 occurred first within platelets which then fragmented under the influence of capillary forces and a large surface/volume ratio. While this study does not provide direct evidence for the transformation path, reported observations strongly suggest that the transformation of δ-Al(Fe,Mn)Si_2 proceeds directly into the α-Al(Fe,Mn)Si phase.

5. Conclusions

Microstructural characterization of the AA6026 alloy in the as-cast state revealed, besides the α-Al(Fe,Mn)Si, the presence of plate-like δ-Al_4(Fe,Mn)Si_2 microconstituents. The δ-Al_4(Fe,Mn)Si_2 phase, morphologically indistinguishable from the more common β-Al_5FeSi, was not expected in wrought 6xxx alloys. Its formation was attributed to the particular combination of the alloying elements: a low Fe/Si ratio that favored the silicon-rich phases and ability of δ-Al_4(Fe,Mn)Si_2 to substitute Fe with Mn and Cr in the alloys with high manganese and chrome content.

Transformation of the metastable δ-Al_4(Fe,Mn)Si_2 occurred at homogenization temperatures as low as 480 °C. It transformed into the α-Al(Fe,Mn)Si phase, which, in turn, underwent fragmentation into a string of particles under the influence of capillary forces. The extent of the fragmentation and spheroidization increased as the homogenization temperature rose from 480 °C to 550 °C. The product of the transformation, α-Al(Fe,Mn)Si, had a primitive cubic lattice, indicating the ordering of Fe and Mn atoms. The dendritic α-Al(Fe,Mn)Si microconstituent also underwent disintegration under capillary effects but preserved the b.c.c. lattice.

Acknowledgement

This work was supported by the Ministry of Science, Technological Development and Innovation of the Republic of Serbia under contract No. 451-03-47/2023-01/200135. The authors would like to thank personnel of the Lab for Atomic Physics - Vinča Institute of Nuclear Sciences facilitating access to their transmission electron microscope.

Author Contributions

T. Radetić: Conceptualization, Methodology, Investigation, Writing-original draft; M. Popović:

Validation, Writing- Review & Editing; M. Novaković: Investigation, Validation; V. Rajić: Investigation, E. Romhanji: Supervision, Resources.

Data Availability

The data are available from the corresponding author upon reasonable request.

Conflicts of Interest

The authors declare no conflict of interest.

References

[1] G. Gosh, in Ternary Alloy Systems: Phase Diagrams, Crystallographic and Thermodynamic Data · Light Metal Systems. Part 2 (G.Effenberg, S. Ilyenko), Springer Materials, Berlin Heidelberg, 2005, p. 359-409.

[2] L. F. Mondolfo, Aluminium Alloys, Structure and Properties, Butter Worths, London, 1979, p. 759.

[3] T. Sheppard, Extrusion of Aluminium Alloys, Kluwer Academic Publishers, Dordrecht/Boston/London, 1999, p. 253.

[4] R. Naddella, D.G. Eskin, Q. Du, L. Katgerman, Macrosegregation in direct-chill casting of aluminium alloys, Progress in Materials Science, 53 (3) (2008) 421-480. https://doi.org/10.1016/j.pmatsci.2007.10.001

[5] H. Tanihata, T. Sugawara, K. Matsuda, S. Ikeno, Effect of casting and homogenizing treatment conditions on the formation of Al-Fe-Si intermetallic compounds in 6063 Al-Mg-Si alloy, Journal of Materials Science, 34 (1999) 1205-1210. https://doi.org/10.1023/A:1004504805781

[6] J.E.Tibballs, J.A. Horst, C.J. Simensen. Precipitation of α-Al(Fe,Mn)Si from the melt, Journal of Materials Science, 36 (2001) 937-941. https://doi.org/10.1023/A:1004815621313

[7] N. Bayat, T. Carlberg, M. Cieslar, In-situ study of phase transformations during homogenization of 6005 and 6082 Al alloys, Journal of Alloys and Compounds, 725 (2017) 504-509.

[8] N. Bayat, T. Carlberg, M. Cieslar, In-situ study of phase transformations during homogenization of 6060 and 6063 Al alloys, Journal of Physics and Chemistry of Solids, 130 (2019) 165-171. https://doi.org/10.1016/j.jpcs.2018.11.013

[9] L. Sweet, S. M. Zhu, S. X. Gao, J.A. Taylor, M.A. Easton, The effect of iron content on the iron-containing intermetallic phases in a cast 6060 aluminum alloy, Metallurgical and Materials Transactions A, 42 (2011) 1737-1749. https://doi.org/10.1007/s11661-010-0595-6

[10] G. Mrówka-Nowotnik, J. Sieniawski, M. Wierzbiński, Intermetallic phase particles in 6082 aluminium alloy, Archives of Materials Science and Engineering, 28 (2) (2007) 69-76. https://doi.org/10.1515/amm-2015-0263

[11] S. Kumar, P.S. Grant, K.A. Q. O'Reilly, Evolution of Fe bearing intermetallics during DC casting and homogenization of an Al-Mg-Si Al alloy, Metallurgical and Materials Transactions A, 47 (2016) 3000-3014. https://doi.org/10.1007/s11661-016-3451-5

[12] K.B.S. Couto, S.R. Claves, W. H. van Geertuyden, W. Z. Misolek, M. Goncalves, Effects of homogenization treatment on microstruvture and hot ductility of aluminium alloy 6063, Materials and Technology, 21 (2) (2005) 263-269. https://doi.org/10.1179/174328405X18584

[13] G. Sha, K. O'Reilly, B. Cantor, J. Worth, R. Hamerton, Growth related metastable phase selection in a 6xxx series wrought Al alloy, Materials Science and Engineering A, 304-306 (2001) 612-616. https://doi.org/10.1016/S0921-5093(00)01545-8

[14] A. Verma, S. Kumar, P.S. Grant, K.A.Q. O'Reilly, Influence of cooling rate on the Fe intermetallic formation in an AA6063 Al alloy, Journal of Alloys and Compounds, 555 (2013) 274-282. https://doi.org/10.1016/j.jallcom.2012.12.077

[15] S. Zajac, B. Hutchinson, A. Johansson, L.O. Gullman, Microstructure control and extrudability of Al-Mg-Si alloys microalloyed with manganese, Materials Science and Technology, 10 (4) (1994) 323-333. https://doi.org/10.1179/mst.1994.10.4.323

[16] Y. Birol, Homogenization of EN AW 6005A alloy for improved extrudability, Metallurgical and Materials Transactions A, 44 (2013) 504-511. https://doi.org/10.1007/s11661-012-1379-y

[17] Y. Birol, The effect of homogenization practice on the microstructure of AA6063 billets, Journal of Materials Processing and Technology, 148 (2) (2004) 250-258. https://doi.org/10.1016/j.jmatprotec.2004.01.056

[18] Y. Birol, Precipitation during homogenization cooling in AlMgSi alloys, Transactions of Nonferrous Metals Society of China, 203 (7) (2013) 1875-1881. https://doi.org/10.1016/S1003-6326(13)62672-2

[19] Y. Wu, J. Xiong, R. Lai, X. Zhang, Z. Guo, The microstructure evolution of an Al-Mg-Si-Mn-Cu-Ce alloy during homogenization, Journal of Alloys and Compounds, 475 (1-2) (2009) 332-338. https://doi.org/10.1016/j.jallcom.2008.07.032

[20] X. Liu, C. Wang, S-Y. Zhang, J-W. Song, X-L. Zhou, M. Zha, H-Y. Wang, Fe-bearing phase formation, microstructure evolution, and mechanical properties of Al-Mg-Si-Fe alloy fabricated by the twin-roll casting process, Journal of Alloys and Compounds, 886 (2021) 161202. https://doi.org/10.1016/j.jallcom.2021.161202

[21] A.L. Dons, The Alstruc homogenization model for industrial aluminium alloys, Journal of Light Metals, 1 (2) (2001) 133-149. https://doi.org/10.1016/S1471-5317(01)00007-4

[22] N. C.W. Kuijpers, F.J. Vermolen, C. Vuik, P.T.G. Koenis, K.E. Nilsen, S. van der Zwaag, The dependence of the β-AlFeSi to α-Al(FeMn)Si transformation kinetics in Al-Mg-Si alloys on the alloying elements, Materials Science and Engineering A, 394 (1-2) (2005) 9-19. https://doi.org/10.1016/j.msea.2004.09.073

[23] N.C.W.Kuijpers, F.J. Vermolen, C. Vuik, S. van der Zwaag, A Model of the β-AlFeSi to α-Al(FeMn)Si Transformation in Al-Mg-Si Alloys, Materials Transactions, 44 (7) (2003) 1448-1456. https://doi.org/10.2320/matertrans.44.1448

[24] N.C.W.Kuijpers, J. Tirel, D.N. Hanlon, S. van der Zwaag, Quantification of the evolution of the 3D intermetallic structure in a 60005A aluminium alloy during a homogenisation treatment, Materials Characterization, 48 (5) (2002) 379-392.

https://doi.org/10.1016/S1044-5803(02)00289-9

[25] G.N. Haidemenopouls, H. Kamoutsi, A.D. Zervaki, Simulation of the transformation of iron intermetallics during homogenization of 6xxx series extrudable aluminum alloys, Journal of Materials Processing and Technology, 212 (11) (2012) 2255-2260. https://doi.org/10.1016/j.jmatprotec.2012.06.026

[26] C.L. Liu, H. Azizi-Alizamini, N.C. Parson, W.J. Poole, Q. Du, Microstructure evolution during homogenization of Al-Mg-Si-Mn-Fe alloys: Modelling and experimental results, Transactions of Nonferrous Metals Society of China, 27 (4) (2017) 747-753. https://doi.org/10.1016/S1003-6326(17)60085-2

[27] O. Engler, T. Schroter, C. Krause, Formation of Intermetallic Particles during Solidificationand Homogenization of Two Al-Mg-Si Alloys, Materials Science and Technology, 39 (1) (2023) 70-84. https://doi.org/10.1080/02670836.2022.2102279

[28] A. Smolej, M. Soković, J. Kopač, V. Dragojević, Influence of heat treatment on the properties of the free-cutting AlMgSiPb alloy, Journal of Materials Processing and Technology, 53 (1-2) (1995) 373–384. https://doi.org/10.1016/0924-0136(95)01994-P

[29] O. Wouters, J.T.M. de Hosson, Lead induced intergranular fracture in aluminum alloy AA6262, Materials Science and Engineering A, 261 (1-2) (2003) 331–337. https://doi.org/10.1016/S0921-5093(03)00521-5

[30] J. Faltus, M. Karlik Hausild, Proc. International Conference on Aluminum Alloys, June 3-7 2012, Pittsburgh, USA, 2013, p. 873-878.

[31] T. Radetić, M. Popović, A. Alil, B. Markoli, I. Naglič, E. Romhanji, Effect of homogenization temperature on microstructure and mechanical properties of Al-Mg-Si alloy containing low-melting point elements, Journal of Alloys and Compounds, 902 (2022) 163719. https://doi.org/10.1016/j.jallcom.2022.163719

[32] S. Yuan, L. Chen, J. Tang, G. Zhao, C. Zhang, J. Yu, Correlation between homogenization treatment and subsequent hot extrusion of Al-Mg-Si alloy, Journal of Materials Science, 54 (2019) 9843-9856. https://doi.org/10.1007/s10853-019-03570-0

[33] F. Alvarez-Antolin, J. Asensio-Lozano, A. Cofino-Villar, A. Gonzales-Pocino, Analysis of different solution treatments in the transformation of β-AlFeSi Particles into α-(FeMn)Si and their influence on different ageing treatments in Al-Mg-Si alloys, Metals 10 (5) (2020) 620. https://doi.org/10.3390/met10050620

[34] M. Quian, J.A. Taylor, J.Y. Yao, M.J. Couper, D.H. StJohn, A practical method for identifying intermetallic phase particles inaluminium alloys by electron probe microanalysis, Journal of Light Metals, 1 (3) (2001) 187-193. https://doi.org/10.1016/S1471-5317(01)00012-8

[35] M.V. Kral, H.R. McIntyre, M.J. Smillie, Identification of intermetallic phases in a eutectic Al-Si casting alloy using electron backscattered diffraction pattern analysis, Scripta Materialia, 51 (3) (2004) 215-219. https://doi.org/10.1016/j.scriptamat.2004.04.015

[36] J. Yu, Formation of intermetallic phases in Al-10Si-0.3Fe based alloys, PhD Thesis, Technische Universitat Berlin, Berlin, 2016.

[37] L.G. Hou, H. Cui, Y.H. Cai, J.S. Zhang, Effect of (Mn+Cr) addition on the microstructure and thermal stability of spray-formed hypereutectic Al-Si alloys, Materials Science and Engineering A, 527 (1-2) (2009) 85-92. https://doi.org/10.1016/j.msea.2009.07.041

[38] H.J. Huang, Y.H. Cai, H. Cui, J.F. Huang, J.P. He, J.S. Zhang, Influence of Mn addition on microstructure and phase formation of spray-deposited Al-25Si-xFe-yMn alloy, Materials Science and Engineering A, 502 (1-2) (2009) 118-125. https://doi.org/10.1016/j.msea.2008.10.005

[39] M. Timpel, N. Wanderka, B.S. Murty, J. Banhart, Three-dimensional visualization of the microstructure development of Sr-modified Al-15Si casting alloy using FIB-EsB tomography using, Acta Materialia, 58 (20) (2010) 6600-6608. https://doi.org/10.1016/j.actamat.2010.08.021

[40] M.V. Kral, P.N.H. Nakashima, D.R.G. Mitchell, Electron microscope studies of Al-Fe-Si intermetallics in an Al-11 Pct Si alloy, Metallurgical and Materials Transactions A, 37 (2006) 1987-1997. https://doi.org/10.1007/s11661-006-0141-8

[41] D.G. Eskin, Physical Metallurgy of Direct Chill Casting of Aluminum Alloys,Taylor & Francis Group, Boca Roton, 2008, p. 50.

[42] G. Sha, K.A.Q. O'Reilly, B. Cantor, J.M. Titchmarsh, R.G. Hamerton, Quasi-peritectic solidification reactions in 6xxx series wrought Al alloys, Acta Materialia, 51 (7) (2003) 1883-1897. https://doi.org/10.1016/S1359-6454(02)00595-5

[43] C. Hsu, K.A.Q. O'Reilly, B. Cantor, R.Hamerton, Non-equilibrium reactions in 6xxx series Al alloys, Materials Science and Engineering A, 304-306 (2001) 119-124. https://doi.org/10.1016/S0921-5093(00)01467-2

[44] S. Cui, R. Mishra, I.-H. Jung, Thermodinamic analysis of 6xxx alloys: phase fraction diagrams, Journal of Mining and Metallurgy, Section B: Metallurgy, 54 (1) (2018) 119-131. https://doi.org/10.2298/JMMB170512052C

[45] L. Yan, Y. Zhang, X. Li, Z. Li, F. Wang, H. Liu, B. Xiong, Microstructural evolution of Al-0.66Mg-0.8Si alloy during homogenization, Transactions of Nonferrous Metals Society of China, 24 (4) (2014) 939-945. https://doi.org/10.1016/S1003-6326(14)63146-0

[46] Y.S. Choi, J.S. Lee, W.T. Kim, H.Y. Ra, Solidification behavior of Al-Si-Fe alloys and phase transformation of metastable intermetallic compound by heat treatment, Journal of Materials Science, 34 (1999) 2163-2168. https://doi.org/10.1016/S0921-5093(00)01467-2

[47] L. Lodgaard, N. Ryum, Precipitation of dispersoids containing Mn and/or Cr in Al–Mg–Si alloys, Materials Science and Engineering A, 283 (1-2) (2000) 144-152. https://doi.org/10.1016/S0921-5093(00)00734-6

[48] J.E. Yoo, A. Shan, I.G. Moon, A study on composition and crystal structure of dispersoids in AlMgSi alloys, Journal of Materials Science, 34 (1999) 2679-2683. https://doi.org/10.1023/A:1004673321013

PREPOZNAVANJE FAZA KOJE SADRŽE Fe U MIKROSTRUKTURI LIVENE LEGURE AA6026 I NJIHOVA EVOLUCIJA TOKOM POSTUPKA HOMOGENIZACIJE

T. Radetić [a,*], M. Popović [a], M. Novaković [b], V. Rajić [b], E. Romhanji [a]

[a] Univerzitet u Beogradu, Tehnološko-metalurški fakultet, Beograd, Srbija
[b] Univerzitet u Beogradu, Institut za nuklearne nauke „Vinča“, Katedra za atomsku fiziku, Nacionalni institut Republike Srbije, Beograd, Srbija

Apstrakt

Ispitivanje prisustva faza koje sadrže Fe u mikrostrukturi livene legure AA6026, kao i njihova evolucija tokom postupaka homogenizacije na temperaturama od 480-550 °C, sprovedena su korišćenjem optičke mikroskopije, skenirajuće elektronske mikroskopije (SEM) i transmisione elektronske mikroskopije (TEM) u kombinaciji sa analizom EDS-a. Osim faze α-Al(Fe,Mn)Si sa dendritskom morfologijom, identifikovane su dve vrste pločastih mikrokonstituenata koji sadrže Fe u mikrostrukturi livene legure. EDS mikroanaliza i elektronska difrakcija pokazali su da jedan skup ploča predstavlja samo tanke sekcije mikrokonstituente α-Al(Fe,Mn)Si. Drugi skup pločastih mikrokonstituenata identifikovan je kao četvrtasta, silicijumom bogata faza δ-Al_4(Fe,Mn)Si_2. Formiranje faze δ-Al_4(Fe,Mn)Si_2 povezano je sa hemijskim sastavom legure. Tokom homogenizacije, metastabilna faza δ-Al_4(Fe,Mn)Si_2 transformisala se u fazu α-Al(Fe,Mn)Si i fragmentirala. Dendritski mikrokonstituenti α-Al(Fe,Mn)Si takođe su fragmentirali. Međutim, dok su mikrokonstituenti α-Al(Fe,Mn)Si sačuvali kubnu kristalnu rešetku tipa b.c.c. tokom procesa, proizvod transformacije faze δ-Al_4(Fe,Mn)Si_2 pokazao je prostu kubnu rešetku.

Ključne reči: *Legure 6xxx; Mikrokonstituenti koji sadrže Fe; Faza δ-Al_4(Fe,Mn)Si_2; Homogenizacija; Fazna transformacija*